OPEN ACCESS

Self-excited motions in dusty plasmas with gradient of charge of macroparticles

New Journal of Physics
An Institute of Physics and Deutsche Physikalische Gesellschaft Journal

Self-excited motions in dusty plasmas with gradient of charge of macroparticles

O S Vaulina[1], A A Samarian[2], O F Petrov[1], B W James[2] and V E Fortov[1]

[1] Institute for High Energy Densities, Russian Academy of Sciences, Izhorskay 13/19, Moscow, 127412, Russia
[2] School of Physics, University of Sydney, NSW 2006, Australia
E-mail: samarian@physics.usyd.edu.au

New Journal of Physics **5** (2003) 82.1–82.20 (http://www.njp.org/)
Received 21 January 2003
Published 2 July 2003

Abstract. Various self-excited motions in dusty plasmas involving spatial variations of macroparticle charge are considered. Two basic types of instabilities in these systems are examined numerically and analytically. The main attention is given to the vortex motions of macroparticles. Conditions suitable for creating the instabilities examined are discussed. Experimental observations of self-excited oscillations in dc-glow, and capacitive rf, discharges are presented. It is shown that spatial variation of dust charge can account for many phenomena observed in inhomogeneous laboratory dusty plasmas.

PII: S1367-2630(03)58566-4

Contents

Introduction

Problems associated with the formation and occurrence of instabilities in dissipative systems of interacting macroparticles are under discussion in various fields of science (plasma physics, molecular biophysics, hydrodynamics, etc) [1, 2]. Dusty plasmas provide a useful experimental model for the study of instabilities in these systems. A dusty plasma consists of electrons, ions, neutral gas atoms or molecules and micron-sized charged dust particles [3]. The combined effect of dissipation in such plasmas and other processes can induce both stationary dust structures (similar to a liquid or solid) and dynamic phenomena (waves, regular or stochastic oscillations) [4]–[11]. Unstable dynamic structures, where steady-state motion is completely determined by the properties of the system and independent of the initial conditions, are of the greatest interest. In many experimental situations, multiple oscillations, vertical vibrations, acoustic waves and other synchronized motions of particles are observed [4, 5, 7, 9, 11]. These have recently appeared in many publications devoted to the analysis of self-excited oscillations of macroparticles [4, 5, 12]–[16]. Some studies address experimental observations of dust vortex motion in various types of plasmas: radio-frequency discharge plasmas [17]–[20], dc-glow discharge plasmas [21]–[23] and nuclear-excited plasmas [24].

Self-excited oscillations in dusty plasma systems differ from oscillations in a conservative system, as there are both dissipative energy losses and external work done via a range of mechanisms. As similar self-excited motions of macroparticles are observed in plasmas generated by different discharges, it is logical to assume that the electrical force is the source of these motions. One possible mechanism capable of transforming the potential energy of an external electric field into kinetic energy of macroparticles is spatial or temporal variation of dust charge [4, 12]–[16, 21]. When emission processes are negligible, the dust particles usually

achieve electrostatic equilibrium with respect to the plasma by acquiring a negative charge. This charge is not fixed but is coupled self-consistently to the surrounding plasma. For this reason, various instabilities can lead to the excitation of dust motion. Nevertheless, the causes of many dynamic phenomena (vortices, combined oscillations) in dusty plasmas are still not sufficiently well understood. For example, random charge fluctuations, which are always present in a dusty plasma, can induce dust 'heating' [13, 25]. These fluctuations, however, cannot explain the occurrence of regular self-excited motions of particles without additional energy sources to compensate for dissipative losses. Here we focus on the systematic variation of dust charge. Such charge variation can be present in dusty plasma systems due to the inhomogeneity of the bulk plasma surrounding the dust cloud, for example, due to the gradients of temperature T_e (T_i) and concentration n_e (n_i). Other reasons for dust charge variation can be spatially varying irradiance or dust surface temperature in the case of macroparticles composed of emitting material [26].

In section 1 of this paper, conditions for inducing self-excited oscillations in systems with spatial variations of macroparticle charge are considered. In section 2, the parameters of the macroparticles in the inhomogeneous plasma of gas discharges are analysed. The results of numerical simulations using molecular Brownian dynamics, focusing on the case of the vortex motion of macroparticles, are presented in section 3. In section 4, the results of experimental observations of self-excited oscillations in dc-glow and capacitive rf discharges are presented. Conditions suitable for inducing instabilities in laboratory dusty plasmas are discussed.

1. Formation of self-excited oscillations in inhomogeneous systems

1.1. Dispersion relations for non-conservative systems

Dispersion relations $L(\omega, \boldsymbol{k}) = 0$ are the linear analogue of differential wave equations of motion and determine the functional dependence of oscillation frequency ω on wavevector $\boldsymbol{k}$. The analysis of the roots $\omega(\boldsymbol{k})$ of the equation $L(\omega, \boldsymbol{k}) = 0$ allows the regime's nontrivial and unstable solutions of the wave equations to be determined. The roots of the dispersion relations $L(\omega, \boldsymbol{k}) = 0$ do not have an imaginary part for conservative systems. The wave equations, which describe the evolution of oscillations in a weakly non-linear limit, describe the competition between non-linearity and dispersion. The non-linear terms produce harmonics (when the initial wave has sufficient amplitude), which compete with dispersion effects, creating the final equilibrium. This situation differs significantly from the case of oscillations in non-conservative systems where there is dispersion of energy, and energy input can occur as a result of a range of mechanisms, including background flows, temperature gradients or charge gradients. In such systems the roots $\omega(\boldsymbol{k})$ of the dispersion relations $L(\omega, \boldsymbol{k}) = 0$ are complex functions $\omega = \omega_R + \mathrm{i}\omega_I$ and the wave solutions have dissipative characteristics: exponentially decreasing for $\omega_I < 0$ and exponentially increasing for $\omega_I > 0$. In the region $\omega_I > 0$, the oscillations will take away energy from the reserves of available potential energy. As a result, the infinitesimal perturbations that appear in a system due to thermal or other fluctuations will grow.

Mathematical models developed for the study of oscillations in non-equilibrium non-linear systems involve the analysis of differential wave equations. In these models there are two basic types of instabilities: (i) dissipative instabilities for systems, where dissipation is present; and (ii) dispersion instabilities, when dissipation is negligibly small [27]. The amplitude $f(A, x, t)$ for an instability of category (i) has a first-order time derivative, while for an instability of category (ii), $f(A, x, t)$ contains a second-order time derivative. The elementary equations for

case (i) are non-linear diffusion equations, which describe some convectional motion, vortexes, dissipative structures and autowaves [27]–[30]. Examples of the equations for case (ii) instability in weakly dissipative systems include the Van der Pole equations, which describe the oscillations of various auto-generators, and the Lorentz system, which is the basic model in the theory of stochastic oscillations [27, 29, 30].

We consider small harmonic perturbations with amplitude $\boldsymbol{b}$ of a stable system G described by a dispersion relation $L(\omega, \boldsymbol{k}) = 0$:

$$\varphi = \boldsymbol{b}\exp\{\mathrm{i}kx - \mathrm{i}\omega t\}. \tag{1}$$

The differential wave equations can be written in functional form as $L(\omega, \boldsymbol{k}) \equiv \det(\hat{G}) = 0$ will determine whether the model under consideration contains decay terms. When attenuation is present (case (i)), $L(\omega, \boldsymbol{k})$ will be a complex function both for stable ($\omega_I < 0$) and for unstable ($\omega_I > 0$) states of the system. The roots of the dispersion relation will also be complex, $\omega = \omega_R + \mathrm{i}\omega_I$, and equation (1) can be written as $\varphi = \boldsymbol{b}\exp\{\mathrm{i}kx - \mathrm{i}\omega_R t\}\exp\{\omega_I t\}$. For $\omega_I > 0$ the solution will increase in time and will be unstable. The point at which the value of ω_I changes sign is the point of bifurcation of the system. For case (ii), the dispersion relation is a real function, but its roots may be a complex conjugate pair: $\omega = \omega_R \pm \mathrm{i}\omega_I$. Equation (1) can be written as $\varphi = \boldsymbol{b}\exp\{\mathrm{i}kx - \mathrm{i}\omega_R t\}\exp\{\pm\omega_I t\}$, and the solution will increase exponentially for any $\omega_I \neq 0$. For stable solutions $\omega_I = 0$, the harmonic perturbation will propagate dispersively instead of attenuating as in a dissipative system.

An important feature of the active medium is the tendency of the system to transfer energy mainly via a mode that corresponds to the bifurcation point of the system. In the case of strong dispersion as a result of the development of instability (ii), only one mode 'survives'. The steady-state motion represents a harmonic wave with a frequency close to the resonant frequency ω_c of the system. In the case of weak dispersion, the form of the steady-state motion can represent impulses of various shapes, which are far from sinusoidal. Notice that, in many physical problems involving simulation of hydrodynamic systems, the insertion of even feeble viscosity destroys the character of, or completely excludes the occurrence of, dispersion solutions.

1.2. Conditions for the occurrence of self-excited oscillations

We will assume that the system consists of N_p charged macroparticles in an electric field of a two-dimensional cylindrical trap with spatial variation of dust charge $Z = Z(r, y) = Z_{oo} + \Delta Z(r, y)$, where $r = (x^2 + z^2)^{1/2}$ is the radial coordinate. We will consider the equation of motion, taking into account the macroparticle's pair interaction F_{int}, the gravitational force $m_p g$, the force due to the electrical field $\vec{E}(r, y) = \vec{i}E(y) + \vec{j}E(r)$, the friction force and the Brownian force F_{br}, produced by the impact of molecules of the surrounding gas:

$$m_p\frac{\mathrm{d}^2\vec{l}_k}{\mathrm{d}t^2} = \sum_j F_{int}(l)\Big|_{\vec{l}=|\vec{l}_k-\vec{l}_j|}\frac{\vec{l}_k - \vec{l}_j}{|\vec{l}_k - \vec{l}_j|} - m_p\nu_{fr}\frac{\mathrm{d}\vec{l}_k}{\mathrm{d}t} + \vec{F}_{br} + \vec{F}_{ext}. \tag{2}$$

Here l is the interparticle distance, m_p is the particle mass, ν_{fr} is the friction frequency, $F_{int}(l) = -eZ(r, y)(\partial\phi_D/\partial l)$, where $\phi_D = (eZ(r, y)/l)\exp(-l/D)$ is the interparticle potential with screening length D, and e is the electron charge. The total external force is equal to $\vec{F}_{ext} = \vec{i}\{E(y)eZ(r, y) - m_p g\} - \vec{j}E(r)eZ(r, y)$. Thus, both the external electric force and the interparticle interaction are dependent upon the particle coordinate. When the curl of these forces is not equal to zero, this system can do positive work, compensating for the dissipative losses of

energy. One can easily see that a simulation of dust dynamics by equations (2) is valid when dust motion does not perturb the external electrical field $\vec{E}(r, y)$, which is the result of the difference in average distributions of concentrations n_e (n_i) of plasma electrons (ions). This will be true for n_e (n_i) $\gg Z_{oo}n_p$, where n_p is the dust concentration and $Z_{oo} \gg \Delta Z(r, y)$. This situation exists, for example, in most cases of gas discharge complex plasmas, where $n_e(n_i) > 2 \times 10^8$ cm^{-3} and $Z_{oo}n_p < 1.6 \times 10^8$ cm^{-3} [4, 5, 7, 9, 10]. Equations (2) will also be applicable for small dust clouds (dust clusters) when the majority of particles are at the edge of the dust structure. For a spherical dust cloud the condition is $N_p < 4^4\pi/3 \approx 260$.

Determination of the conditions for the occurrence of dust oscillations for the system described by equations (2) is practically impossible. In the one-dimensional case, the problem can be reduced to a nonlinear partial differential equation [27, 29]. However, this transformation is extremely laborious for solving spatial problems and requires additional assumptions on the nature of the interparticle interaction. Therefore we have restricted the analysis to a two-dimensional equation of motion for a single particle in a gravity field, in an external electric field and in an aggregate internal electric field due to the charged particles of the dust cloud:

$$\vec{E}^{int}(r, y) = \vec{i}E^i_y(r, y) + \vec{j}E^i_r(r, y) \equiv \sum_j \frac{\partial\phi_D}{\partial l}\Big|_{l=|\vec{l}_k-\vec{l}_j|} \frac{\vec{l}_k - \vec{l}_j}{|\vec{l}_k - \vec{l}_j|}.$$

We have assumed that the Brownian force and the collective effects, which are connected with spatial fluctuations of charges of other macroparticles in a dust cloud, play a negligible role at the onset of instability.

Suppose that a particle with charge $Z_o = Z_{oo} + \Delta Z(r_o, y_o)$ is in a stable state at an extreme point in the dust cloud in the position (r_o, y_o) relative to its centre, and we shall consider its response to some displacement to (r, y) from the point of equilibrium (r_o, y_o). We denote the first derivatives of parameters at the point (r_o, y_o) as $\alpha_r = \mathrm{d}E^e(r)/\mathrm{d}r$, $\alpha_y = -\mathrm{d}E^e(y)/\mathrm{d}y$, $\gamma_r = \partial E^i_r(r, y)/\mathrm{d}r$, $\gamma_y = \partial E^i_y(r, y)/\mathrm{d}y$, $\beta_r = \partial Z(r, y)/\mathrm{d}r$, $\beta_y = \partial Z(r, y)/\mathrm{d}y$ and $\gamma_o = \partial E^i_r(r, y)/\mathrm{d}y \equiv \partial E^i_y(r, y)/\mathrm{d}r$, which is valid because $\mathrm{rot}\vec{E}(r, y)$ is equal to zero for the case of $Z(r, y) =$ constant. The linearized version of equations (2) for small particle displacement can be written as [28]

$$\frac{\mathrm{d}^2r}{\mathrm{d}t^2} = -\nu_{fr}\frac{\mathrm{d}r}{\mathrm{d}t} + a_{11}r + a_{12}y, \tag{3a}$$

$$\frac{\mathrm{d}^2y}{\mathrm{d}t^2} = -\nu_{fr}\frac{\mathrm{d}y}{\mathrm{d}t} + a_{22}y + a_{21}r, \tag{3b}$$

where $a_{11} = -eZ_o\{a_r - \gamma_r\}/m_p$, $a_{12} = \pm eZ_o\gamma_o/m_p$, $a_{22} = [-eZ_o\{\alpha_y - \gamma_y\} + m_pg\beta_y/Z_o]/m_p$, $a_{21} = [\pm eZ_o\gamma_o + m_pg\beta_\rho/Z_o]/m_p$ for the case of the stationary stable state of the dust particle ($r_o = r(t \to \infty)$; $\pm y_o = y(t \to \infty)$; $E^e(r_o) = E^i_r(r_o, \pm y_o)$; $E^e(y_o) \pm E^i_y(r_o, \pm y_o) = m_pg/eZ_o$) in a position above the centre of the dust cloud $(r_o, +y_o)$ or under it $(r_o, -y_o)$. Equations (3*a*) and (3*b*), a system of linearized amplitude equations (see section 1.1) without spatial gradients [27, 28], can be used to determine the conditions for instability. We obtain a 'dispersion relation' $L(\omega) \equiv \det(\hat{G}) = 0$ from the response of the system to a small perturbation $\varphi \sim \exp\{-\mathrm{i}\omega t\}$, which arises in the direction r or y:

$$\omega^4 + (a_{11} + a_{22} - \nu^2_{fr})\omega^2 + (a_{11}a_{22} - a_{12}f_{21}) + \mathrm{i}\nu_{fr}\omega\{2\omega^2 + f_{11} + f_{22}\} = 0. \tag{4}$$

Equation (4) determines an area of existence of nontrivial and unstable solutions in the system $\hat{G}(-\mathrm{i}\omega; \mu)b$, described by equations (3*a*) and (3*b*). The detailed analysis of relation (4) was

presented in [12]. This analysis has shown that the small perturbations in system (3*a*) and (3*b*) will grow in two cases: (i) when a restoring force is absent, and (ii) near some characteristic resonant frequency ω_c of the system, when the frictional force does not damp sufficiently the oscillating motion.

The occurrence of dissipative instability type (i) is determined by the condition

$$(a_{11}a_{22} - a_{12}a_{21}) \leq 0. \tag{5}$$

The equality in equation (5) determines a neutral curve of the dissipative instability ($\omega_R = 0, \omega \equiv \omega_I = 0$). Taking into account the value of the coefficients a_{ij}, and assuming that $Z_o \approx Z_{oo} \gg \Delta Z(r, y)$, we can obtain

$$eZ_o\{(\alpha_\rho - \gamma_\rho)(\alpha_y - \gamma_y) - \gamma_o^2\} < \frac{\gamma_o \beta_r g}{Z_o}. \tag{6}$$

As $(\alpha_\rho - \gamma_\rho)\{\alpha_y - \gamma_y\} > \gamma_o^2$, the left part of equation (6) is positive and the system is stable for $\beta_r = 0$. The sign of the right side of the inequality is determined by the signs of γ_o and β_r. For the case of $\beta_r > 0$, a particle located below the centre of the dust cloud ($\gamma_o < 0$) is unstable, and for $\beta_r < 0$, the instability will take place only for particles located in the upper part of the system. As the second derivative with respect to time can be neglected, and $\vec{\Omega} = \mathrm{rot}(\vec{V})$, where $\vec{V}$ is the particle velocity, which is not equal to zero, the condition (6) describes the occurrence of dust vortex motions along a closed curve. The direction of dust rotation in a vertical plane for monotonic spatial dependencies of $\vec{E}(r, y)$ and $Z(r, y)$ can be obtained from the sign of $\Omega = g\beta_r/\{Z_o \nu_{fr}\}$ in the linearized equations (3*a*) and (3*b*). For $\Omega > 0$ the particles will move downwards in the centre of the dust cloud and upwards for $\Omega < 0$. It should also be noted that condition (6) is independent of friction (ν_{fr}). Thus the occurrence of type (i) instability is determined by the topology parameters of the system: the value Z_o, the radial gradients β_r of the particle charges, their concentrations n_p and the form of the dust cloud.

The characteristic which distinguishes the dispersion instability (ii) from the dissipative bifurcation (i) is a strong dependence on the friction coefficient ν_{fr}. The reduction of ν_{fr} leads to perturbations with frequencies ω close to a natural resonant frequency ω_c (where $\omega_c^2 = |a_{11} + a_{22}|/2$) of the system. The occurrence of type (ii) instability ($\omega = \omega_R \pm \mathrm{i}\omega_I$) will be determined by

$$\omega_c^2 \leq \frac{4a_{12}a_{21} + (a_{11} - a_{22})^2}{4\nu_{fr}^2}. \tag{7}$$

In the case of strong dispersion, as a result of the development of type (ii) instability, the steady-state motion typically represents a harmonic oscillation with a frequency close to the bifurcation point of the system ω_c [27]. Thus the dispersion spectrum of the motion takes place close to the resonant frequency ω_c when the friction in the system is balanced by incoming potential energy. In the general case, oscillations with frequency ω_c will develop, when dissipation does not destroy the structure of the dispersion solution ($\nu_{fr} < \omega_c$) and does not allow considerable shifts of the neutral curve, where $\omega_I = 0$. For amplification of the oscillating solutions, it is necessary that [12, 27]:

$$\nu_{fr} < \omega_c < \omega_\Omega = \frac{|\Omega|}{2}. \tag{8}$$

Equation (8) determines the region of dispersion instability, where, under the condition of synchronized motion of separate particles in a dust cloud, solutions similar to waves are possible.

It is necessary to note that the inequality (8) is not a criterion for the occurrence of dispersive instability because the ω_Ω value is an upper estimate of ω_c, which determines the position of the neutral curve in some special cases ($a_{11} \cong a_{22}$) [12]. For estimating the frequency of steady-state oscillations we can use the value $\omega_c \approx \omega_\Omega$.

In summary we note that the analysis of the development of instabilities presented in this section is rather approximate because it is based on a considerable simplification of the problem as we did not take into account the spatial gradients, the Brownian force and collective effects. However, this analysis shows qualitatively the presence of two different bifurcations in the cloud of charged macroparticles. To test the viability of our deductions for the conditions close to the experimental ones, we present in section 2 estimates of the parameters of macroparticles in a gas discharge plasma, and in section 3 the results of computer simulations for the complete system of equation (2).

2. Characteristics of a dust system in gas discharge plasmas

2.1. Effect of inhomogeneous plasma parameters on the dust charge

Here we consider conditions close to those in gas discharge plasmas. In the case of $a \leq \lambda_m$, where a is the dust radius and λ_m is the free-path length of molecules in a gas, the friction frequency ν_{fr} can be written in the free-molecular approximation [31]:

$$\nu_{fr}\ (\mathrm{s}^{-1}) \cong C_v P\ (\mathrm{Torr})/(a\ (\mu\mathrm{m})\ \rho\ (\mathrm{g\ cm}^{-3})), \tag{9}$$

where ρ is the dust mass density, P is the gas pressure and C_v is a constant which is determined by the background gas (as examples, $C_v \approx 600$ for neon and $C_v \approx 820$ for argon at room temperature ~300 K). In gas discharge plasmas emission processes are negligible and the equilibrium charge $\langle Z \rangle$ of the dust particles is negative as a result of the higher mobility μ_e of the electrons. Assuming that drift electron (ion) currents are less than thermal ones, $T_i \approx 0.03$ eV and $n_e \approx n_i$, we have, on the basis of orbit motion limited (OML) theory [32],

$$\langle Z \rangle = C_z a\ (\mu\mathrm{m})\ T_e\ (\mathrm{eV}). \tag{10}$$

Here the value of C_z is 2×10^3 for Ar as the background gas. Thus in the case of $Z(r, y) = \langle Z \rangle + \Delta_T Z(r, y)$, where $\langle Z \rangle$ is the equilibrium dust charge at a point in the plasma with electron temperature T_e, and $\Delta_T Z(r, y)$ is the variation of dust charge due to the T_e changes (ΔT_e), we obtain

$$\frac{\Delta_T Z(r, y)}{\langle Z \rangle} = \frac{\Delta T_e(r, y)}{T_e} \qquad \text{and} \qquad \frac{|\beta_y|}{\langle Z \rangle} = \frac{1}{T_e}\frac{\partial T_e}{\partial y}, \qquad \frac{|\beta_r|}{\langle Z \rangle} = \frac{1}{T_e}\frac{\partial T_e}{\partial r}.$$

We now consider the spatial variations $\Delta_n Z(r, y)$ of the equilibrium dust charge, which can occur due to gradients of concentrations $n_{e(i)}$ in the plasma surrounding the dust cloud. Assuming that the conditions in the plasma are close to electroneutral, $\delta n = n_i - n_e \ll n_e \approx n_i \approx n$ and $\Delta_n Z(r, y) \ll \langle Z \rangle$, where $\langle Z \rangle$ is the equilibrium dust charge assuming $n_e = n_i$. Then the value of $\Delta_n Z(r, y)$ can be determined by equating the orbit-limited currents of electrons (ions) for an isolated spherical particle with an equilibrium surface potential $\phi_s < 0$, that is

$$\Delta_n Z(\rho, y) \approx -\frac{\langle Z \rangle \delta n}{n(1 + e^2 \langle Z \rangle / a T_e)} \approx -0.26 \langle Z \rangle \frac{\delta n}{n}, \tag{11}$$

where $\langle Z \rangle \approx 2000a\ (\mu\mathrm{m})\ T_e\ (\mathrm{eV})$ (see equation (10)). For Maxwellian electrons (ions), and $e\varphi(r, y)/T_{e(i)} \ll 1$, we can obtain $\delta n \sim \varphi(r, y)$, where $\varphi(r, y)$ is the potential of the electrostatic

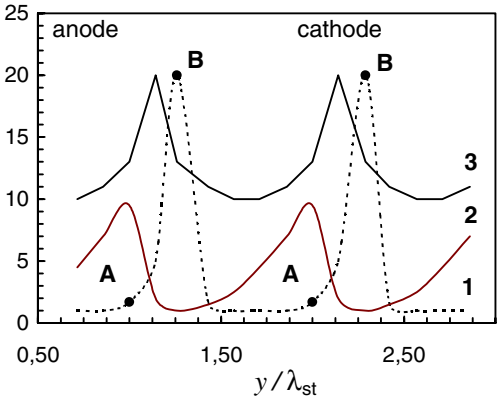

Figure 1. Relative changes of $E(y)/E^o$ (1), of n_e/n_e^o (2) and $10T_e/T_e^o$ (3) versus y/λ_{st} for a striated dc discharge in neon (Ne) with PR = 2.7 cm Torr, $\lambda_{st} \approx 7$ cm. Here n_e^o, T_e^o and E^o are the values of the parameters in the tail of the striation.

field E. Thus in this case the particle charge $Z(r, y)$ will be proportional to the potential $\varphi(r, y)$. This assumption is sometimes used for numerical simulations and for estimating dust charge variations [21, 33, 34]. In the more general case the $\Delta_n Z(\rho, y)$ value can be obtained from the Poisson equation ($\delta n \equiv \text{div}\,\vec{E}/4\pi e$).

As an example we will perform an analysis of inhomogeneous conditions in a striated dc-glow discharge. Measurements of some plasma parameters were presented in [35] for a dc discharge in neon (Ne) with $PR = 2.7$ cm Torr and $\lambda_{st} \approx 7$ cm, where R is the radius of the discharge tube and λ_{st} is the wavelength of the striations (figure 1). The qualitative behaviour of these parameters (n_e, T_e, $E(y)$) corresponds to the results obtained by different authors for striated dc discharges in inert gases [36]–[38]. The levitation of macroparticles in the laboratory plasma is usually observed in regions of high electric field (at the head of the striations, see (A, B) in figure 1), which are close to the region of the brightest luminescence. The value of $\delta n(y)/n \sim D^2/\Lambda^l L_{st}$, where $D = \sqrt{T_e/4\pi e^2 n}$ is the screening length, Λ^l is the typical electron energy relaxation length (Λ^l_{Ne} (cm) $\cong 10/P$ (Torr) for neon) and $L_{st} \sim 1$–3 cm is the length of the region of steepest changes of the electric field. Thus $\Delta_n Z(r, y)/\langle Z\rangle = 0.26(\delta n/n) \ll 1$ is negligibly small compared to $\Delta_T Z(r, y)/\langle Z\rangle = \Delta T_e(r, y)/T_e$, which can achieve values of ~0.5–1. Hence the variation of dust charges in the y direction is determined by the electron temperature gradient and can be considerable in this case: ($|\beta_y|/\langle Z\rangle = (1/T_e)\partial T_e/\partial y \sim 0.5$–$1$ cm^{-1}). In contrast, in the r direction $\partial T_e/\partial r$ is close to zero and the value of $\Delta Z(r, y)/\langle Z\rangle$ will be determined by the radial variation of δn.

In the case of a diffusion-controlled discharge ($R \gg D$) the radial electric field can be written as $E(r) \approx -(T_e/en_e)\partial n_e/\partial r \sim T_e/eR$ [37]. For steady state conditions, the densities of electron (ion) currents $j_{e(i)} = n_{e(i)}V_{e(i)}$ satisfy the equation $\text{div}(j_{e(i)}) = q_{e(i)}$, where $V_{e(i)}$ is the velocity and $q_{e(i)}$ is the source of the electrons (ions). Assuming that diffusion losses of particles are balanced by ionization processes ($q_e \equiv q_i$) and taking into account that, in the case of ambipolar diffusion $V_i = V_e$, we obtain from the Poisson equation: $E(r) \equiv T_e/e\Lambda =$ constant and $\delta n/n \cong -D^2/r\Lambda$. Here $\Lambda \sim R/2.4$ is the characteristic diffusion length, which is determined by the boundary conditions to within a factor of 2 [37]. It should be noted that a more precise solution is not justified, because the basic conclusions of the theoretical model

for ambipolar diffusion are based on neglecting quantities of the order of $\delta n/n$. In the case of $R = 3$ cm, $r > D$ and $D < 1000$ μm, the ratio $\Delta_n Z(r, y)/\langle Z\rangle \approx -0.62(D^2/rR)$ will be less than 3%. Thus the condition $\Delta Z(r, y) \ll \langle Z\rangle$ (used in the derivation of equation (11)) is valid. In this case the dust charge gradient in the radial direction can be estimated from $\beta_r/\langle Z\rangle \cong 0.26D^2/r^2\Lambda \sim 0.002$–$0.22$ cm^{-1}, for $r/D \sim 1$–10 and $\Lambda \approx R/2.4$. Thus β_r is positive and decreases with increasing r. It should be noted that the resulting reduction of β_r with increasing of r is in agreement with the known experimental approximation for the potential, $\phi(r) \sim r^{\alpha}(1 < \alpha < 2)$, of the radial electric field near the centre of dc discharges [22, 38].

2.2. *Kinetic energy of macroparticles*

One of the important questions in the study of motion in non-conservative systems is the amount of energy the steady-state oscillations can receive from the background. As all steady-state motion of charged dust particles in an electrical trap are finite, their kinetic energy for some direction x will be determined by the amplitude A and the characteristic frequency ω:$\langle K_x\rangle \approx m_p A^2\omega^2/2$. Linear analysis does not allow the amplitude A of the steady-state oscillations to be obtained and is applicable only at the initial stages of the motion, when the perturbations are small. The amplitude of the developed vortex oscillations (i) can be estimated taking into account the scale of the steady-state motion $l_p < A < L/2$, where $l_p = n_p^{-1/3}$ is the mean interparticle distance and L is the characteristic size of the dust cloud, the value of which is usually about ∼0.5–2.5 cm. As the stable rotation of particles following the development of dissipative bifurcation (i) has to be described by a diffusion equation, the angular velocity of rotation will limited by the frictional force ($\omega^2 \sim 1/\nu_{fr}^2$). For the case of a linear variation of dust charges $Z(r) \sim Z_{oo} + \beta_r r$ within the trajectory of particle motion, the value ω^2 can be taken as equal to $\Omega^2 = (g\beta_r/Z_{oo}\nu_{fr})^2$. Then the kinetic energy $K_{(i)}$, which is gained by the dust particle after the development of instability (i), can be written in the form

$$K_{(i)} = \frac{m_p g^2 \xi^2}{8\nu_{fr}^2}, \tag{12}$$

where $\xi = \{A\beta_r/Z_{oo}\}$ determines the relative changes of $Z(r)$ within the limits of the trajectory of the particle motion. Thus for the case of $a = 5$ μm, $\rho = 2$ g cm^{-3}, ν_{fr} (s^{-1}) $\cong 60P$ (Torr) (Ne, equation (9)) and $P \sim 0.2$ Torr, we find, that the energy $K_{(i)}$ is one order of magnitude higher than the thermal dust energy $T_o \approx 0.02$ eV at room temperature for $\xi > 10^{-3}$ ($\beta_r/Z_{oo} > 0.002$ cm^{-1}, $A = 0.5$ cm). With increasing gas pressure up to $P = 5$ Torr, or with decreasing particle radius to $a = 2$ μm, the value of $K_{(i)}/T_o > 10$ for $\xi > 10^{-2}$ ($\beta_r/Z_{oo} > 0.02$ cm^{-1}, $A = 0.5$ cm). This estimate shows that even small variations of dust charge can lead to the effective conversion of potential energy from background sources to the kinetic energy of dust motion.

In the case of dispersive instability (ii), the kinetic energy $K_{(ii)}$ of macroparticles can be estimated from the known resonance frequency ω_c. As the transport characteristics of a strongly correlated dust system are determined by the dust frequency

$$\omega_p \cong eZ(r, y)\sqrt{\frac{2n_p \exp(-k)(1 + k + k^2/2)}{m_p}} \tag{13}$$

where $k = l_p/D$ and $Z(r, y) \approx \langle Z \rangle$ for small charge variations, we can assume that the resonance frequency ω_c of the steady-state particle oscillations will be close to ω_p. Then the kinetic energy $K_{(ii)}$ can be written in the form

$$K_{(ii)}\ (\mathrm{eV}) \approx \frac{5.76 \times 10^3\ (a\ (\mu\mathrm{m})\ T_e\ (\mathrm{eV}))^2 \chi^2 c_n}{l_p\ (\mu\mathrm{m})} \tag{14}$$

where $c_n = \exp(-k)\{1 + k + k^2/2\}$ and $\chi = A/l_p$. The value χ is less than 0.5 for a dust cloud with a structure close to that of a solid [12]. Then for the case of $a = 5\ \mu$m, $\chi = 0.1$, $k \approx 1$–2, $l_p = 500\ \mu$m and $T_e \sim 1$ eV, the kinetic energy $K_{(ii)} \approx 3$ eV. The maximum kinetic energy, which is not destroying the crystalline dust structure, is reached at $\chi = 0.5$ and is equal to $K_{(ii)}^{lim} = c_n e^2 \langle Z \rangle^2 / 4 l_p$.

The value of $K_{(ii)}$ can be estimated from equation (12) under the assumption that the steady-state oscillation is similar to the frequency corresponding to the bifurcation point of system (section 1.2, equation (8)). Nevertheless the exact determination of frequency ω for steady-state dust motion using linear analysis is not possible for most practical cases. A possible reason, which influences considerably the value of ω, is the various collective effects associated with the interparticle interaction. These effects can lead to the development of new types of instabilities or play a phenomenologically dissipative role in restricting ω. The spatial fluctuations of surrounding particles can change the oscillation frequency of an individual particle or lead to the stochastization of its motion. It is necessary to emphasize, however, that the appearance of a regular motion as a result of the instabilities considered is a special case of the solution of the non-linear differential equations. When the random forces F_{ran} which arise do not have a correlation with the Brownian force F_{br}, the kinetic temperature T_s of the dust system will grow ($T_s = T_o + \Delta T$) and its increase will be determined by $\Delta T \sim \langle F_{ran}^2 \rangle / \nu_{fr}(\nu_{fr} + \eta)$, where η is the characteristic frequency of the random force action F_{ran} [13].

3. Numerical simulation for systems with charge gradients of macroparticles

3.1. Parameters of the problem

For the solution of the three-dimensional problem (see section 1.2, equation (2)) the method of Brownian dynamics was used [12]. The external electric fields were assumed to be linear $\vec{E}^{ext}(r, y) = \vec{i}(E_G + \alpha_y y) + \vec{j}\alpha_r r$. The charge variation was given by $Z(r, y) = Z_{oo}(1 + \beta_r^* r^2 + \beta_y^* y^2)$, with the change in particle charge not exceeding 30% within the dust cloud. For all cases the dust temperature T_o was ~0.03 eV, $D \cong 1000\ \mu$m and the radial gradient $\alpha_r \cong 3 N_p^{-1/3}$ V cm^{-2}. The parameters β_r^*, β_y^* were varied proportionally as $N_p^{-2/3}$. The friction frequency ν_{fr} and the relation of the gradient α_y (of the electric field in the direction of gravity) to the radial gradient α_r were also varied. Some numerical results for systems containing from 15 up to 3000 particles are presented below. Under the chosen conditions, various cases of dynamic equilibrium motion were observed: vortices, regular oscillations and stochastic motion. A mean interparticle distance l_p, determined as a maximum of the pair correlation function, was from 500 to 2300 μm. The dynamic behaviour of macroparticles was dependent on the characteristic frequencies ν_{fr}, ω_p and on the angular frequency ω_Ω (equation (8)). It should be noted that a replacement of the square-law dependence of $Z(r, y)$ by linear or cubic functions does not change the qualitative character of the particle motion or its dependence on the value of ν_{fr}.

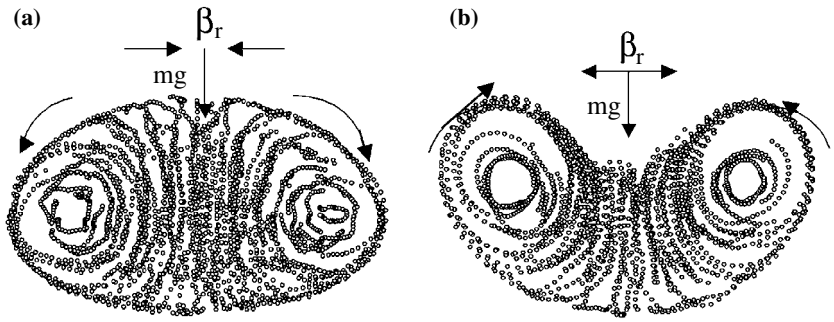

Figure 2. Examples of dust vortex motion (trajectories of particles for the time interval $t \sim 150/\nu_{fr}$) for systems with the different parameters: (a) $\nu_{fr} \cong 77\ \mathrm{s}^{-1}$, $\alpha_y/\alpha_r = 2, Z_{oo} = 4\times10^4, \beta_r^* \cong -2\ \mathrm{cm}^{-2}, \beta_y^* = 0$; (b) $\nu_{fr} \cong 115\ \mathrm{s}^{-1}, \alpha_y/\alpha_r = 1$, $Z_{oo} = 8 \times 10^3, \beta_y^* = \beta_r^* \cong 5.5\ \mathrm{cm}^{-2}$.

3.2. Vortex motions of macroparticles

In contrast to turbulent vortex motion, which is a special case of stochastic self-excited oscillations, regular vortices such as periodic circular, spiral or concentric motions can be observed in non-linear systems. Examples of two different cases of synchronized quasi-harmonic motion for small dust clusters are given in figures 2(a), (b). In the first case (figure 2(a), $N_p = 15$) the calculations were performed for a radial charge gradient $Z(r) = Z_{oo}(1 + \beta_r^* r^2)$, where $Z_{oo} = 4 \times 10^4$, $\beta_r^* \cong -12.5 N_p^{-2/3}\ \mathrm{cm}^{-2}$ and $Z_{oo}/m_p \cong 10^{15}\ \mathrm{g}^{-1}$. The mean interparticle distance corresponded to $k = l_p/D \cong 2, \omega_p \cong 77\ \mathrm{s}^{-1}$. In the second case (figure 2(b), $N_p = 25$), the calculations were performed for $Z(r, y) = Z_{oo}(1 + \beta_r^* r^2 + \beta_y^* y^2)$, where $Z_{oo} = 8 \times 10^3$ ($Z_{oo}/m_p \cong 2 \times 10^{14}\ \mathrm{g}^{-1}$) and $\beta_y^* \equiv \beta_r^* \cong 50 N_p^{-2/3}\ \mathrm{cm}^{-2}$. The mean interparticle distance corresponded to $k = l_p/D \cong 1.6, \omega_p \cong 115\ \mathrm{s}^{-1}$.

With increasing $N_p > 60$, the parameters of the dust motion approached the parameters of large-scale low-frequency oscillations (the oscillations with amplitude greater than l_p). For all cases, the character of the steady-state motion did not depend on the starting conditions or on the initial spatial ordering of macroparticles. The stability of small cluster systems was broken with decreasing asymmetry of the dust cloud ($\alpha_y/\alpha_r \to \sqrt{2}$), and also with increasing β_r^* or N_p up to 100. For further increases of N_p, the dynamic characteristics of the dust system did not vary significantly.

The conditions for the excitation of rotation were independent of the frictional force (ν_{fr}) and the value of β_y^*. While the direction of particle rotation was determined by the coefficient β_r^*, the amplitude was almost independent of ν_{fr}. The rotation frequency varied inversely with the friction coefficient ν_{fr} and the mean kinetic energy of macroparticles $\langle K \rangle \sim 1/\nu_{fr}^2$. With decrease of ν_{fr} below some critical value $\nu_{lim} \approx 0.1$–$0.15\omega_p$, randomization of the dust motion occurred (the dust trajectories become complicated and irregular and the number of harmonics with similar amplitudes increase). The time dependence of the oscillation amplitude of an individual particle is given in figure 3 for the different friction frequencies. The distribution of particle velocities become more uniform in each direction ($\langle K_y \rangle \approx \langle K_x \rangle = \langle K_z \rangle$) and are similar to a Maxwellian function with temperature $T_s \approx \frac{2}{3}\langle K \rangle$.

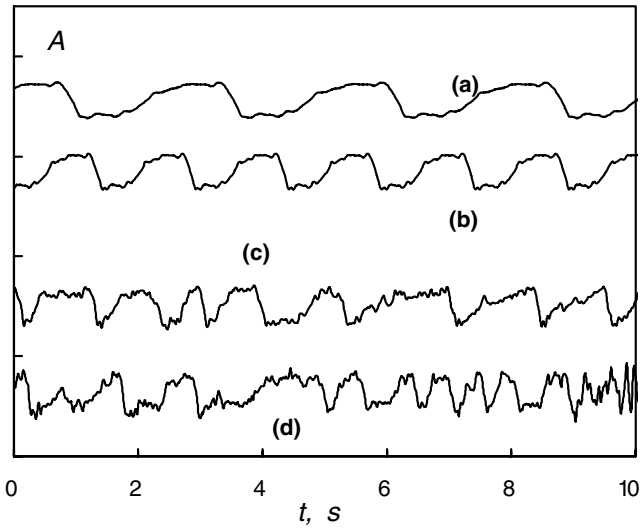

Figure 3. The dependence of oscillation amplitude of an individual particle in the vertical direction is shown as a function of time for the different friction frequencies: (a) $\nu_{fr} \cong 77\ \mathrm{s}^{-1}$; (b) $\nu_{fr}/2$; (c) $\nu_{fr}/6$; (d) $\nu_{fr}/10$.

3.3. Examples of the 'dispersive motion' of macroparticles

We consider two examples of a possible dust motion in the case of instability (ii), which can provide a qualitative explanation of some effects observed in experiments such as the acoustic oscillations or the 'abnormal heating' of macroparticles [11, 21, 25, 39, 40]. The calculations were carried out for systems consisting of from 15 up to 60 macroparticles. The requirement of small N_p is critical as, in this case, criteria (7) and (8) can be easily realized for conditions close to those for the formation of dissipative instability, without an excitation of vortex motions. The example of self-excited regular motion, similar to acoustic oscillations, is given in figures 4(a)–(c).

The parameters of the system are specified in the caption to the figure. The difference between these parameters and those for the problem described in section 3.2 is the choice of α_y/α_ρ value, which characterizes the form of the dust cloud (see figure 2). The mean interparticle distance corresponded to $k = l_p/D \cong 2.3$, $\omega_p \cong 52\ \mathrm{s}^{-1}$. Self-excited motion of particles occurred for $\nu_{fr} < \nu_c \cong 1\ \mathrm{s}^{-1}$. The frequency ω_c and the amplitude of the steady-state oscillations were almost independent of ν_{fr} with decreasing ν_{fr} until $\nu_{lim} \cong 0.38\ \mathrm{s}^{-1}$. When ν_{fr} approaches ν_{lim} appreciable differences in the phases of the motion of individual particles were observed. Decreasing frequency ν_{fr} below the threshold ν_{lim} produced a rapid heating of the system, followed by pumping and explosion.

As a result of the destruction of the vertical alignment of particles due to insignificant changes of the system parameters or due to external action on the dust cloud, the motion of particles becomes irregular (see figure 5(b)). The spatial ordering of the dust particles is one of the basic requirements for the development of harmonic motions in the dust cloud. The trajectories of particles after development of a bifurcation in a system of reoriented particles ($\nu_{fr} < \nu_c \cong 4\ \mathrm{s}^{-1}$, $\omega_p \approx \omega_\Omega \cong 55\ \mathrm{s}^{-1}$) are presented in figure 5(b) for $\nu_{fr} \cong 1.5\ \mathrm{s}^{-1}$. The velocity distributions are isotropic and close to the Maxwellian function with the temperature $T_s \approx \frac{2}{3}\langle K \rangle$ (see figure 5(c)).

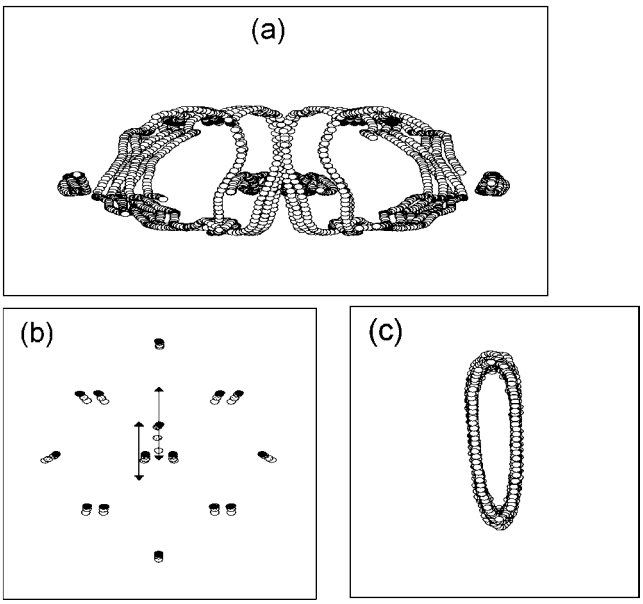

Figure 4. Side view for $\nu_{fr} > 1\ \mathrm{s}^{-1}$ (a), trajectories of particles for the time interval $t \sim T/2 = 2\pi/\omega$ and for $\nu_{fr} \cong 1\ \mathrm{s}^{-1}$ (b) and an enlarged section (c) for the trajectory of an individual particle for the case of (b) in the dust system with $\alpha_y/\alpha_r = 0.4$, $Z_{oo} = 4 \times 10^4$, $\beta_r^* \cong -2\ \mathrm{cm}^{-2}$, $\beta_y^* = 0$.

The kinetic energy $\langle K \rangle$ of particles varies with ν_{fr}; as ν_{fr} decrease from $4\ \mathrm{s}^{-1}$ up to $2\ \mathrm{s}^{-1}$, $\langle K \rangle$ increases from $2.5T_o$ up to $20T_o$. On the one hand, this can be produced by a correlation between the random induced electrical forces and the Brownian motion of particles. On the other hand, the dependence of $\langle K \rangle$ on ν_{fr} can reflect a sequence of different bifurcations occurring with decreasing ν_{fr}. As already mentioned above, one of the basic models of a stochastic motion is a Lorentz system, the solutions of which are irregular functions of time over a wide parameter range. As a result of a small change in the parameters of this system, its solutions become so complex, that it led to chaos. In the computer analysis of the dust velocities this effect will resemble an increase in the kinetic temperature of the macroparticles.

4. Experimental observations of the self-excited motions of macroparticles in gas discharges

Theoretical analysis and numerical simulation show that in plasmas with gradients of dust charge, various dust particle motions can be excited. Many experiments show that the dust structures observed in rf-discharge plasmas are more stable than dust structures observed in dc-discharge plasmas. In this section, using the proposed model, we analyse the conditions for the occurrence of different self-excited dust motions in the striation region of a dc-glow discharge and in a capacitive rf discharge. We attribute the observed instabilities to inhomogeneities in the plasma and show that greater instability of dust structures in dc discharges can be explained by larger space charge gradients in such plasmas.

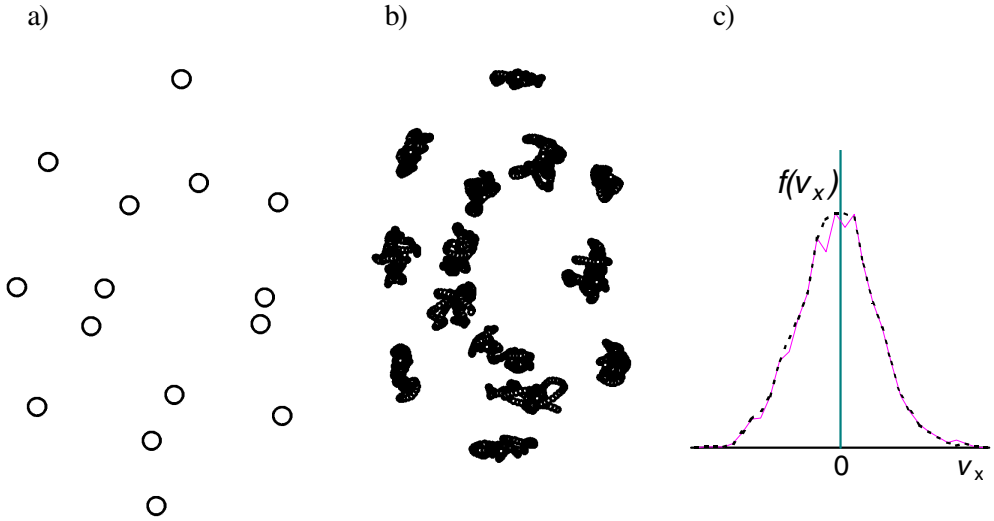

Figure 5. Side view for $\nu_{fr} > 4\ \mathrm{s}^{-1}$ (a), trajectories of particles for the time $t \sim 150/\nu_{fr}$ and for $\nu_{fr} \cong 1.5\ \mathrm{s}^{-1}$ (b) and the dust velocity distributions $f(V_x)$ (full curve) (c) in the dust system with $\alpha_y/\alpha_r = 0.41$, $Z_{oo} = 4 \times 10^4$, $\beta_r^* \cong -2\ \mathrm{cm}^{-2}$, $\beta_y^* = 0$. The broken curve in figure 4(c) is the Maxwellian function with $T_s = 2\langle K_x \rangle \approx 1$ eV.

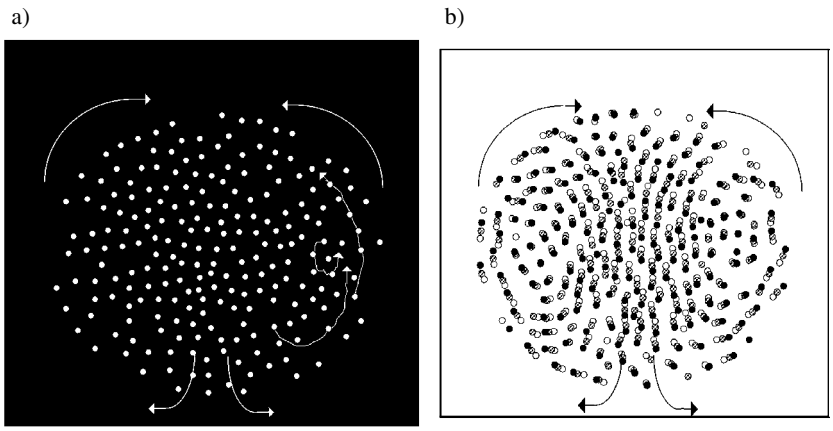

Figure 6. Digital images of dust convection (a) in the striation of a dc-glow discharge and (b) results of numerical simulations.

4.1. Experiments in the dc-glow discharge

The experiment was carried out in a standard dc-discharge tube. A detailed description of the experimental procedure can be found in [7]. Video images of self-excited dust motion in the striations of dc discharges are shown in figures 6–8. Experiments were carried out in argon (Ar) at pressures in the range $P = 0.1$–1 Torr and discharge currents $I = 0.5$–15 mA, with iron particles of radius $a \cong 3.5\ \mu$m ($\rho = 8\ \mathrm{g\ cm}^{-3}$).

A digital image of convection in a dust cloud is shown in figure 6(a). The direction of dust rotation (indicated by arrows) shows that $\Omega > 0$ ($\beta_r > 0$), in accordance with the

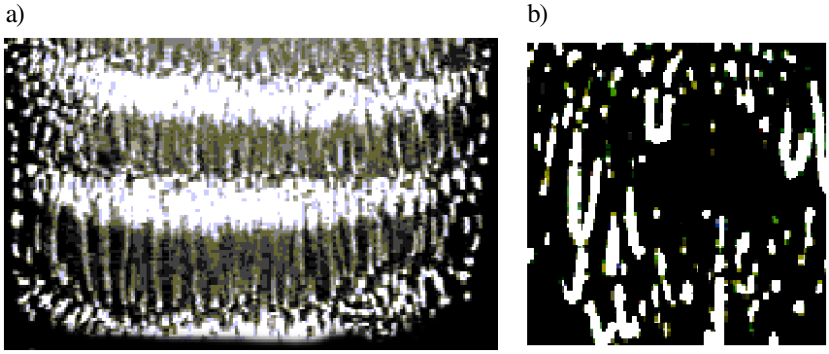

Figure 7. Video image of dust compressive waves (a) and an enlarged section (b) of trajectories of individual particles.

theoretical analysis presented in section 2. An experimental estimate of β_r can be made from the measurement of velocities $V = A\Omega/2$ and the diameter A of dust rotation. Thus we obtain $\beta_r/\langle Z\rangle = 2V\nu_{fr}/Ag \approx 0.01$ cm^{-1} (ν_{fr} (s^{-1}) $\cong 30P$ (Torr) $\cong 24$ s^{-1}, $P = 0.8$ Torr, equation (9)), in accordance with the theoretical predictions (see section 2). The results of numerical simulations are presented in figure 6(b) for the problem described by equation (2) with parameters close to the experimental ones ($N_p = 3000$, exposure time $t_{ex} \approx 0.5$ s). The calculated mean kinetic energy of the dust particles ($\langle K\rangle \sim 4.5 \times 10^{-18}$ J) agrees with the experimentally measured value.

Dust longitudinal compressive waves are shown in figure 7(a). Although the large-scale dust motions constitute longitudinal waves, the individual particles in the dust cloud move in small-scale elliptic trajectories (figure 7(b)) similar to the simulated ones (see figure 4(c)). The size of ellipses, and thus the oscillation amplitude, decreases towards the boundaries of the dust cloud. This can be explained by the decreasing value of β_r in the r direction, which was mentioned above, or can be connected with collective effects similar to those obtained in numerical simulations (see figure 4(b)). The frequency ω of oscillations in the centre of the cloud was ∼45–50 s^{-1}. Assuming $\omega = \Omega/2 \approx g\beta_r/2Z_{oo}\nu_{fr}$, $\nu_{fr} \cong 9$ s^{-1} ($P = 0.3$ Torr), we obtain $\beta_r/\langle Z\rangle \cong 0.8$–$0.9$ cm^{-1}.

The difference between this value of β_r and the numerical estimates (see section 2.1) can be explained by the low time resolution (∼1/25 s) of measurements that prevent reliable tracing of fast individual particles within the same trajectories. Another reason for a high value of β_r may be related to the possible loss of ions and electrons in the region of the dust cloud, leading to a decrease in the characteristic diffusion length Λ (section 2.1), which can cause an increase in the electric field $E(r)$ and, correspondingly, the β_r value. It should be mentioned that the analysis presented above was performed leaving out of account spatial derivatives (see section 3.3). Thus we cannot expect it to give a fully detailed and quantitative description of the dust waves. For further analysis the proposed model has to be completed by equations including the spatial gradients.

The rotation of macroparticles in the upper part of a dust cloud, in combination with oscillations in the lower part, is typical for a dc-glow discharge [21, 41]. The present mechanism can easily explain these complicated motions, based only on the assumption of different charge gradients in the various regions of a striation. Thus, the observed complex motion (see figure 8) can be considered as a simultaneous occurrence of two types of instabilities (i) and

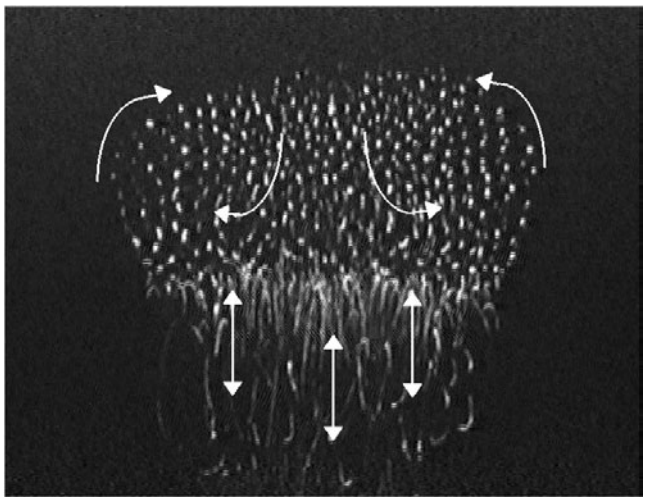

Figure 8. Complex self-excited motions of macroparticles in the striations of a dc-glow discharge.

(ii) in different parts of the dust cloud. Assuming that $2\pi e^2\langle Z\rangle \exp(-k)/l_p^2 \approx E$, where $E \cong 2.4T_e/eR$, one can exclude the unknown T_e ($\langle Z\rangle \sim T_e$) and estimate $k = l_p/D$ for the different parts of the cloud. For the bottom of the dust cloud ($k \approx 0.8$, $l_p \approx 800$ μm) we have $D \approx 1000$ μm. The observed frequency of oscillations was $\omega \sim 30$–40 s^{-1}, whence we can obtain $\beta_r/\langle Z\rangle = 2\omega\nu_{fr}/g \sim 0.27$–$0.37$ cm^{-1} for $\nu_{fr} \cong 4.5$ s^{-1} ($P = 0.15$ Torr). In the upper part of the cloud ($k \approx 2$, $l_p \approx 450$ μm), the screening length D decreases to 225 μm. In the last case the measured ratio of $V/A \approx 0.25$ s^{-1} gives the following experimental estimate: $\beta_r/\langle Z\rangle = 2V\nu_{fr}/Ag \approx 0.002$ cm^{-1}.

The values obtained for D are in agreement with the increase of n_e in the upper part of the cloud (see figure 1) from 10^8 to 10^9 cm^{-3} for $T_e \approx 1$–2 eV [37, 38]. On the other hand, the ratio β_r for the different parts of the dust cloud is not proportional to D^2 (see section 2.1). There are a number of reasons for this, the most evident of which is the occurrence of type (i) instability (in the upper part of the structure) for particles close to the edge of the dust cloud, where the γ_o value is sufficiently large. In contrast, the occurrence of type (ii) instability (in the bottom of the structure) is determined by the particles inside the dust cloud, where the value of β_r can be much larger, as shown above. It is necessary to add that all the self-excited motions of dust particles considered are also observed in inductive rf discharges, which have non-uniform characteristics similar to those of dc discharges [42].

4.2. Production of the self-excited oscillations in the capacitive rf discharges

There are two fundamental reasons which prevent the development of type (i) and (ii) instabilities in capacitive rf discharges. The first is the homogeneity of the plasma, while the second is concerned with the small number of layers of macroparticles observed and, consequently, with the small shift parameter γ_o (see section 1). This explains the absence of experimental observations of vortex motion in normal circumstances. Nevertheless, the formation of bulk dust clouds, for example in microgravity, or the introduction of an extra electrode leads to the occurrence of dissipative instability (i), which caused the convection of dust particles [18, 19, 23]. One

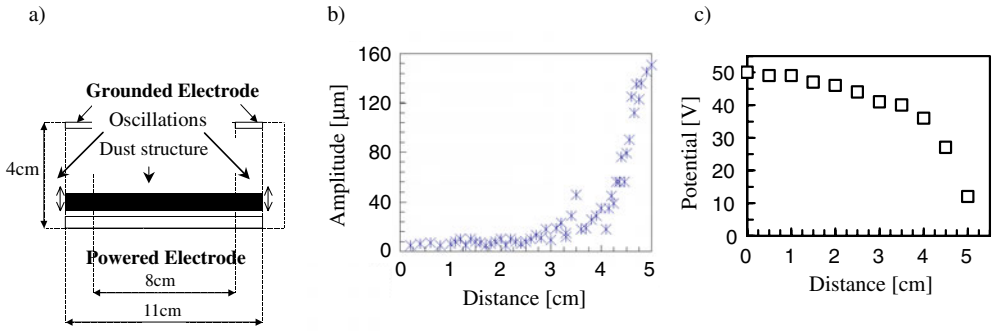

Figure 9. Simplified schematic diagram (a) of experiments in an rf discharge, (b) the radial profile of the oscillation amplitude and (c) of the electric field potential ($h = 11$ mm).

example of the dispersive instability (ii) in a capacitive rf discharge may be the observation of self-excited oscillations in one-dimensional layers of dust particles [4, 5].

Here we present some experimental examples of the occurrence of dispersive and dissipative instabilities in planar capacitive rf discharges. A schematic diagram of the experiment is shown in figure 9(a). Experiments were carried out in argon (Ar) at pressures $P = 0.120$ Torr, with melamine formaldehyde particles ($a \cong 1.4$ μm ($\rho = 1.5$ g cm^{-3})). We used an aluminium disc as the powered electrode and a stainless steel ring as the grounded electrode. The diameters of the electrodes were 10 cm for the disc and 11 cm for the ring. The powered electrode was placed below the grounded ring. In our experiments the ring is centred on the axis of the system and the distance between the electrodes was 50 mm. The input power was 65 W and the resulting dc self-bias of the powered electrode was 35 V, measured at the electrical feedthrough. The laser beam entered the discharge chamber through a 40 mm diameter window. A window mounted on a side port in a perpendicular direction allowed a view of the light scattered at 90° by the suspended dust particles and provided a vertical cross section of the dust structure. In addition, we used the top window to view the horizontal dust structure. The laser beam could be expanded in the vertical and horizontal directions into sheets of light by a system of cylindrical lens. Images of the illuminated dust cloud were obtained using a charged-coupled device (CCD) camera with a 60 mm micro-lens. The video signals are stored on a videotape recorder or were transferred to a computer via a frame-grabber card with an 8-bit grey scale and 640 × 480-pixel resolution. The coordinates of particles were measured in each frame and individual particles were traced from one frame to the next.

The experiment used a multilayer structure which filled the whole discharge region as shown in figure 9(a). Such structures can be created by embedding a large number of dust particles (more than 10^5) in the discharge. It was found that, for a wide range of conditions, the central part of the structure is stable but there are spontaneous oscillations of particles near the edge of the electrode ($r > 4$ mm). The radial profile of the oscillation amplitude is shown in figure 9(b). From the analysis above we suggest that these oscillations occurred in the region where the value of the dust charge gradient β_r is largest. This increase in β_r can be associated with a steep gradient of the potential $\phi(r)$ of the radial electric field near the edge of the powered electrode [37]. The results of radial profile $\phi(r)$ measurements 11 mm above the electrode are presented in figure 9(c). One can see that $\phi(r)$ is weakly dependent on r near the centre of the powered electrode. Assuming $\phi(r) \sim \ln(r)$ gives $E(r) \sim 1/r$ from the solution of the Poisson

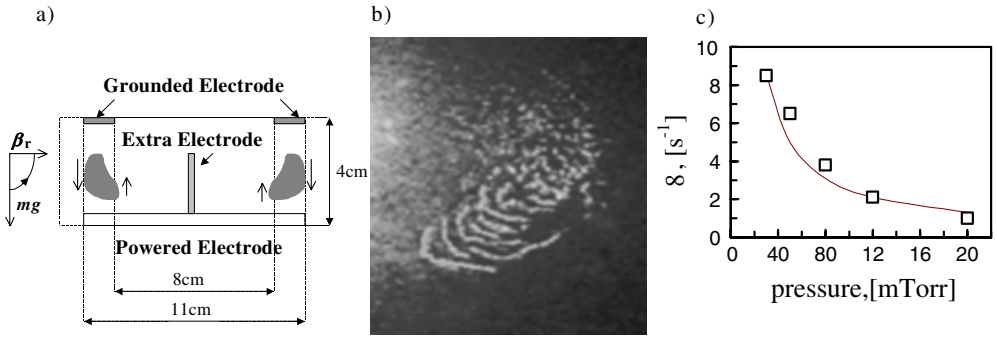

Figure 10. The vertical dust rotations in an rf discharge: (a) a simplified schematic diagram of the experiments; (b) the video images of self-excited dust motions; (c) the dependence of rotation frequency ω on pressure.

equation, and correspondingly $\beta_r \sim 0$. Near the edge of the electrode the dramatic increase of $\phi(r)$ leads to positive derivatives $(\partial E(r)/\partial r,\ \partial^2 E(r)/\partial r^2)$ of the electric field, and as a result $\partial\delta n/\partial r > 0$, and $\beta_r < 0$. It should be noted that decreasing electron temperature near the edge of the electrode [37] could also play an important role in the decrease of dust charge in this case.

Another kind of instability can occur in the presence of an extra electrode at the centre of the powered electrode. In this case displacement of dust particle structure d from the centre of the electrode towards the edge and self-excited vertical vortex motion is observed. The simplified schema of experiments on the formation of a dust cloud with the help of an extra electrode is shown in figure 10(a). A video image of a dust vortex observed in this case is shown in figure 10(b). The direction of dust rotation is in accordance with $\Omega < 0$ (in contrast to the cases observed in dc discharge, see figures 6 and 8). This allows us to assume that the charge gradient β_r is negative for this case too, i.e. the edge particles have a smaller charge. The dependence of dust rotation frequency ω on pressure is presented in figure 10(c). For our experimental condition the friction frequency can be written in a free-molecular approach as $\nu_{fr}\ (\mathrm{s}^{-1}) \cong 200P$ (Torr) [24]. Assuming $\omega = \Omega/2 \approx g\beta_r/\{2\langle Z\rangle\nu_{fr}\}$, we can obtain the value of $\beta_r/\langle Z\rangle \approx 0.1\ \mathrm{cm}^{-1}$ from fitting the experimental data (see figure 10(c)). This value is an order of magnitude less than the charge gradient for the dc-discharge plasma, but on the other hand this is two orders of magnitude more that one usually finds in planar rf discharges.

5. Conclusions

We have considered two basic types of instabilities (dissipative and dispersive) in a dust system with spatial charge variations. The conditions for occurrence of these instabilities have been studied. The results of the analysis can be easily adapted to any non-conservative system, for which linearized equations have a similar form. The occurrence of dissipative instability depends on the topological characteristics of the system and is independent of the viscosity of the surrounding gas. As a result of this instability, the dust vortex motion similar to ring oscillations, spiral waves or to convection can be observed. The conditions for the occurrence of the dispersive instability are related to a decrease in frictional forces. This instability can induce regular oscillations or stochastic dust fluctuations, which can lead to the 'heating' of the dust along with temporal charge variations. These self-excited motions result from the same

mechanism, but for the formation of regular oscillations synchronization of the motions of the individual macroparticles is necessary. Numerical simulations of the dust systems in an external electric field and gravitational field have shown that both regular oscillations and stochastic fluctuations can self-excite as the result of the instabilities considered. For the occurrence of these self-excited motions, large spatial variations of dust charges are not required. Even a small charge gradient in the dust cloud ($\sim$1%) is an effective source of kinetic energy for the dust particles.

Results of experimental observations of different self-excited oscillations in dc-glow and rf discharges were presented. Numerical estimates show that the existence of these oscillations can be explained by the occurrence of dust charge gradients provided by the disturbance of electroneutrality in the experimental plasma devices. The importance of the proposed mechanism for the occurrence of self-excited dust motions is that it provides a possible explanation for a considerable range of phenomena ('abnormal dust heating', vortices, regular oscillations) which are observed in laboratory dusty plasmas, without the need for other mechanisms or background sources of energy.

Acknowledgments

This work was supported by the Russian Foundation for Basic Research, grant 01-02-16658, INTAS no 2000-522, Australian Research Council and the Science Foundation for Physics within the University of Sydney. AAS was supported by a University of Sydney U2000 Fellowship. The authors would like to thank Dr A Chernyshev for assistance in conducting the dc-discharge experiment and Mr W Tsang for assistance in conducting the rf-discharge experiment.

References

[1] Gaponov-Grekhov A V 1992 *Nonlinearities in Action* (Berlin: Springer)
[2] Strogatz S H 1994 *Nonlinear Dynamics and Chaos* (Reading, MA: Addison-Wesley)
[3] Tsytovich V N 1997 *Sov. Phys.–Usp.* **40** 53
[4] Nunomura S, Misawa T, Ohno N and Takamura S 1999 *Phys. Rev. Lett.* **83** 1970
[5] Samarian A A, James B W, Vladimirov S V and Cramer N F 2001 *Phys. Rev.* E **64** 025402(R)
[6] Merlino R L, Barkan A, Thompson C and D'Angelo N 1998 *Phys. Plasmas* **5** 1067
[7] Samarian A A *et al* 2001 *Sov. Phys.–JETP* **92** 454
[8] Wang Y, Juan W and Lin I 2000 *Phys. Rev.* E **62** 5667
[9] Molotkov V I *et al* 1999 *Sov. Phys.–JETP* **89** 477
[10] Samsonov D and Goree J 1999 *Phys. Rev.* E **59** 1047
[11] Thomas E Jr and Watson M 1999 *Phys. Plasmas* **6** 4111
[12] Vaulina O S, Nefedov A P, Petrov O F and Fortov V E 2000 *Sov. Phys.–JETP* **91** 1063
[13] Vaulina O S, Khrapak S A, Nefedov A P and Fortov V E 1999 *Phys. Rev.* E **60** 5959
[14] Shukla P K 2000 *Phys. Lett.* A **268** 100
[15] Ivlev A V, Konopka U and Morfill G 2000 *Phys. Rev.* E **62** 2739
[16] Fortov V E *et al* 2000 *Phys. Plasmas* **7** 1374
[17] Chiang Chi-Hui and Lin I 1996 *Phys. Rev. Lett.* **77** 647
[18] Low D A, Steel W H, Annaratone B M and Allen J E 1998 *Phys. Rev. Lett.* **80** 4189
[19] Morfill G *et al* 1999 *Phys. Rev. Lett.* **83** 1598
[20] Vaulina O S, Samarian A A, Nefedov A P and Fortov V E 2001 *Phys. Lett.* A **289**
[21] Zhakhovskii V V *et al* 1997 *JETP Lett.* **66** 392

[22] Zhakhovskii V *et al* 1998 *FNTP-98: Proc. on Physics of Low Temperature Plasma (Petrozavodsk, Russia, 1998)* (PetroUni) p 684
[23] Uchida G, Izuka S and Sato N 2001 *ICPP-2000: Proc. 10th Int. Congress on Plasma Physics (Quebec City, Canada, 2000)* vol 2 (Boury-Royal de Beauport) p 416
[24] Fortov V *et al* 1999 *Phys. Lett.* A **258** 305
[25] Quinn R A and Goree J 2000 *Phys. Rev.* E **61** 3033
[26] Ostrikov K N, Yu M Y and Stenflo L 2000 *Phys. Rev.* E **61** 782
[27] Dodd R K, Eilbeck J C, Gibbon J and Morris H C 1982 *Solitons and Nonlinear Wave Equations* (New York: Academic)
[28] Nicolis G and Prigogine I 1977 *Self-Organization in Non-Equilibrium Systems* (New York: Wiley)
[29] Akhromeeva T, Kurdyumov S and Malinetskii G 1988 *Computers and Nonlinear Phenomena* (Moscow: Nauka)
[30] 1998 *Physical Encyclopedia* vol 1 (Moscow: Bol'shaya Rossiiskaya Entsiklopediya) pp 11, 15, 654
[31] Landau L and Lifshitz Y 1970 *Course of Theoretical Physics* (Oxford: Pergamon)
[32] Goree J 1994 *Plasma Sources Sci. Technol.* **3** 400
[33] Antipov S N, Samarian A A, Petrov O F and Nefedov A P 2001 *Plasma Phys. Rep.* **27** 342
[34] Ma J X, Liu J and Yu M Y 1997 *Phys. Rev.* E **55** 4627
[35] Golubovskii Yu B and Nisimov S U 1995 *Zh. Tekh. Fiz.* **65** 46
[36] Nedospasov A V 1968 *Usp. Fiz. Nauk* **94** 439
[37] Raizer Y P 1991 *The Physics of Gas Discharge* (Berlin: Springer)
[38] Golubovskii Y *et al* 2000 *Phys. Rev.* E **62** 2707
[39] Melzer A, Homann A and Piel A 1996 *Phys. Rev.* E **53** 2757
[40] Thomas H and Morfill G 1996 *Nature* **379** 806
[41] Fortov V E, Molotkov V I, Nefedov A P and Petrov O F 1999 *Phys. Plasmas* **6** 1759
[42] Usachev A and Mitchell L 2000 private communication